minerals

MDPI

Article

Petrogenetic Implications of the Lithium-Rich Tongtianmiao Granite Pluton, South China: Evidence from Geochemistry and Geochronology

Xinhui Yu [1,2,3], Yongzhang Zhou [1,2,3], Wei Cao [1,2,3,*], Hanyu Wang [1,2,3], Can Zhang [1,2,3], Lifeng Zhong [4], Wu Wei [4], Zhiqiang Wang [5], Jianying Yao [6], Zhiqiang Chen [6] and Qinghe Xu [7]

1 School of Earth Sciences and Engineering, Sun Yat-sen University, Zhuhai 519000, China; yuxh29@mail2.sysu.edu.cn (X.Y.); zhouyz@mail.sysu.edu.cn (Y.Z.); wanghy327@mail2.sysu.edu.cn (H.W.); zhangc68@mail2.sysu.edu.cn (C.Z.)
2 Centre for Earth Environment and Resources, Sun Yat-sen University, Zhuhai 519000, China
3 Guangdong Provincial Key Lab of Geological Process and Mineral Resources, Zhuhai 519000, China
4 Southern Marine Science and Engineering Guangdong Laboratory (Zhuhai), Zhuhai 519000, China; zhonglifeng@sml-zhuhai.cn (L.Z.); weiwu@sml-zhuhai.cn (W.W.)
5 School of Earth Sciences and Spatial Information Engineering, Hunan University of Science and Technology, Xiangtan 411201, China; wangzhiq0218@hnust.edu.cn
6 Mineral Resources Investigation Institute of Hunan Province, Changsha 410083, China; yaojianying870217@163.com (J.Y.); chenzq202@163.com (Z.C.)
7 Hunan Dazhonghe Lithium Mine Co., Ltd., Chenzhou 423000, China; hbjlsxqh@126.com
* Correspondence: caow25@mail.sysu.edu.cn

Abstract: The South China Block, a region renowned for its extensive granite distribution and rich metal deposits, serves as a natural laboratory for the study of granite-related mineralization. This research focuses on the Tongtianmiao granite pluton, which is located at the intersection of the Qin-Hang and Nanling metallogenic belts and has been confirmed as a significant lithium mineral resource. Despite its discovery and ongoing development, the lithium-rich Tongtianmiao pluton has been understudied, particularly concerning its petrogenesis, which has only recently come to the forefront of scientific inquiry. By integrating an array of petrogeochemical data with geochronological studies derived from zircon and monazite dating, this study provides insights into the magmatic processes related to lithium enrichment in the Tongtianmiao granites. The Tongtianmiao granites are classified as A-type granites characterized by high SiO_2 contents (69.18–78.20 wt.%, average = 74.08 wt.%), $K_2O + Na_2O$ contents (4.59–8.34 wt.%, average = 6.86 wt.%), A/CNK > 1.2, and low concentrations of Ca, Mg, and Fe. These granites are enriched in alkali metals such as Li, Rb, and Cs but are significantly depleted in Ba, Sr, and Eu. They show no significant fractionation of light or heavy rare-earth elements but present characteristic tetrad effects. A finding of this study is the identification of multiple ages from in situ zircon U–Pb dating, which implies a prolonged history of magmatic activity. However, given the high uranium content in zircons, which could render U–Pb ages unreliable, emphasis is placed on the monazite U–Pb ages. These ages cluster at approximately 172.1 ± 1.1 Ma and 167.9 ± 1.6 Ma, indicating a Middle Jurassic period of granite formation. This timing correlates with the retreat of the Pacific subduction plate and the associated NE-trending extensional fault activity, which likely provided favorable conditions for lithium enrichment. The study concluded that the Tongtianmiao granites were formed through partial melting of crustal materials and subsequent underplating by mantle-derived materials, and were contaminated by strata materials. This process resulted in the formation of highly differentiated granite through magmatic differentiation and external forces. These findings have significant implications for understanding the petrogenesis of lithium-rich granites and are expected to inform future exploration endeavors in the Tongtianmiao pluton.

Keywords: highly differentiated granite; Tongtianmiao pluton; petrogenesis; geochemistry; U–Pb dating

check for updates

Citation: Yu, X.; Zhou, Y.; Cao, W.; Wang, H.; Zhang, C.; Zhong, L.; Wei, W.; Wang, Z.; Yao, J.; Chen, Z.; et al. Petrogenetic Implications of the Lithium-Rich Tongtianmiao Granite Pluton, South China: Evidence from Geochemistry and Geochronology. *Minerals* **2024**, *14*, 637. https://doi.org/10.3390/min14070637

Academic Editor: Basem Zoheir

Received: 29 April 2024
Revised: 17 June 2024
Accepted: 18 June 2024
Published: 21 June 2024

Copyright: © 2024 by the authors. Licensee MDPI, Basel, Switzerland. This article is an open access article distributed under the terms and conditions of the Creative Commons Attribution (CC BY) license (https://creativecommons.org/licenses/by/4.0/).

1. Introduction

In recent years, there have been significant advancements in understanding the petrogenesis and lithium mineralization mechanisms of lithium-rich granites. Experimental petrology has provided new insights into the role of volatile components (Li, H_2O, CO_2, etc.) and their solubility in silicate melts, which are critical for the formation of rare metal ores. Notably, melts with high Li contents exhibit low viscosity, favoring large crystal growth and influencing rare metal mineral solubility [1,2]. Volatile components within the melt (such as F, B, and P) exhibit a significant affinity for rare metal elements such as Li. These volatiles can alter the composition of the melt, thereby affecting the solubility of rare metal minerals through processes of aggregation or disaggregation [3,4], and ultimately form complexes with these elements, which facilitates their migration and enrichment [5]. In China, significant progress has been made in the research on granite-type lithium deposits, as detailed by Guo et al. (2024) [6], who characterized 40 significant granite-type lithium deposits nationwide and proposed that the formation of pegmatite shells, magmatic fractionation, and dike emplacement are evidence of the gradual ascent of ore-bearing residual melts within the magma chamber.

As the world's largest consumer of lithium, enhancing China's domestic lithium resource supply capacity is of strategic significance. The recent discovery of the Tongtianmiao granite-type lithium deposit in the Xianghualing ore field, which was found by the Mineral Resources Investigation Institute of Hunan Province, revealed a close association between the lithium deposit and the semiburied, highly fractionated granite. Despite considerable geological research accumulated in the Xianghualing ore field, studies have predominantly focused on the petrogenesis [7], diagenetic dynamic background [8], geochemical characteristics [9–11], geochronology [12–15] and rare-metal mineralization [11,16,17] of the Laiziling and Jianfengling plutons, which are also located within the field. Occasionally, some research has also briefly addressed the Tongtianmiao pluton, but these studies have typically been confined to surface-level sampling [17,18]. Consequently, there is currently a lack of detailed research on the vertical distribution and deep characteristics of lithium-bearing granite in Tongtianmiao. This gap is particularly evident when considering the distinctive geological context of granite, which offers a unique opportunity to illuminate the intricate processes of petrogenesis. This study aims to bridge these gaps by integrating comprehensive petrogeochemical data and precise geochronological analyses. We utilize state-of-the-art techniques such as LA–ICP–MS, which have become the benchmark for highly precise dating tools providing unprecedented accuracy and detail. By leveraging these techniques, we aim to conduct a comprehensive and meticulous analysis of the whole-rock major and trace element compositions, alongside in situ U–Pb dating of zircon and monazite from the Tongtianmiao pluton. This study will not only shed light on the ore-forming processes of lithium-rich granites but also provide practical guidance for the assessment and exploration of lithium resources in the area.

2. Geological Background

The Tongtianmiao pluton, located within the South China Block, has recently been identified as a significant lithium resource. The South China Block was formed by the collision of the Yangtze and Cathaysia blocks (Figure 1), which underwent multiple episodes of tectonic–magmatic events and crustal material reorganization since the Neoproterozoic era [19–21]. During the Late Mesozoic to Cenozoic, the region was subjected to the influences of Pacific, Eurasian, and Indian tectonic systems, which contributed to a highly complex geological structure with intense intracontinental mobilized mineralization processes [22–24]. This region serves as a significant base for rare metal deposits in China, with notable enrichment of W, Sn, Li, Be, Ni, Ta, and weathering crust-type rare-earth elements that have attracted global attention [25–27].

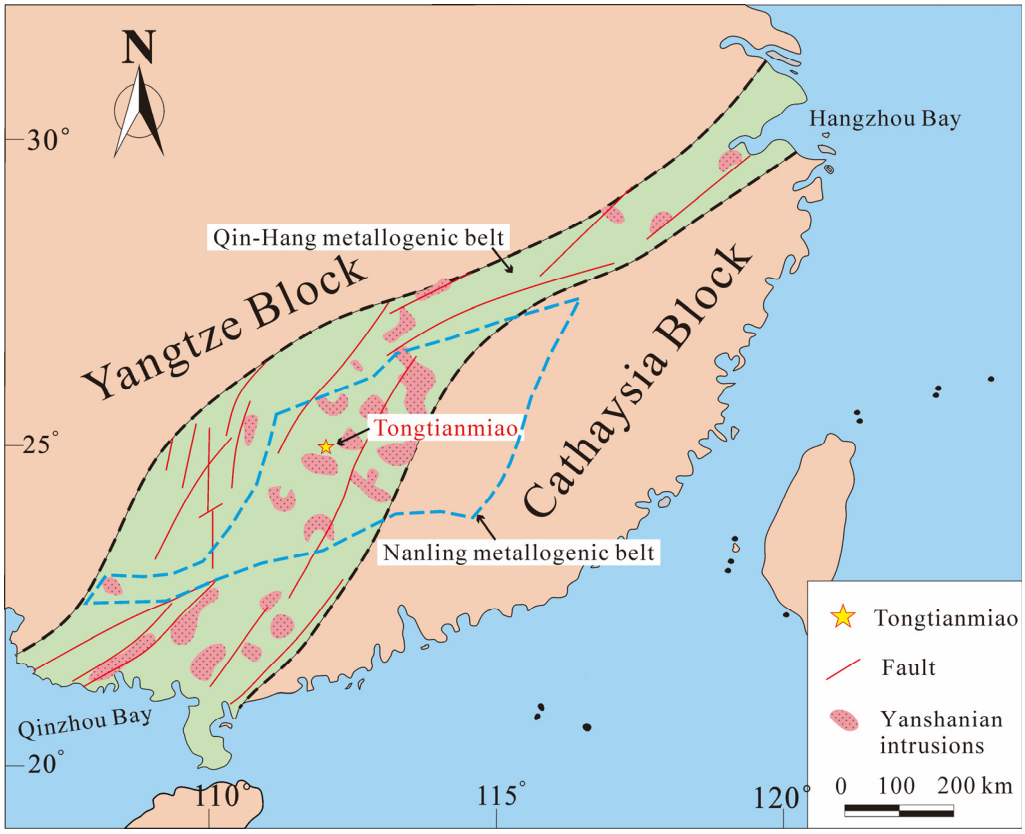

Figure 1. Geological sketch map of the South China Block (modified from Chen et al., 1989 [28], Zhou et al., 2012 [21]), showing the distribution of Yanshanian granitic plutons. The map is presented in the WGS84 coordinate system.

The Tongtianmiao pluton lies in the southern part of Hunan Province, overlapping the Qin-Hang (Qinzhou Bay–Hangzhou Bay) metallogenic belt and the Nanling metallogenic belt, serving as a traditional multimetal resource base for tungsten and tin in China. The mineralization of nonferrous metal resources in the region is closely related to the Mesozoic Yanshanian granite [29–31]. The Tongtianmiao pluton is located on the southeast side of the Chenzhou-Linwu northeast-trending fault within the Xianghualing tin-polymetallic ore field. The exposed strata in the area span from the Cambrian to the Cretaceous, with the Caledonian orogeny (corresponding to the Cambrian to Silurian period) forming a nearly east–west-trending basement structural framework and the Indosinian movement period (corresponding to the Permian to Triassic period) mainly forming a north–south-trending structural framework. The superposition of these two stages of tectonic movement made the Cambrian strata the core of the Tongtianmiao dome anticline (Figure 2). Subsequently, the Yanshanian movement (corresponding to the Jurassic to Cretaceous period) was mainly characterized by the formation of north–northeast- and northeast-trending fault structures, accompanied by a suite of magmatic intrusions. The Yanshanian movement period was the most active in terms of mineralization activities in the region, with the closest relationship between structure and mineralization, serving as the main ore-bearing and ore-hosting structures in the area. The mineralization of rare metal resources in this region is intimately linked to the distribution of granite bodies. Among the exposed plutons, the Laiziling pluton is notably associated with tungsten–tin mineralization [11,12,18,32]; the Jianfengling pluton shows a strong correlation with lithium–niobium–tantalum mineralization [7,8,33,34]; and ongoing lithium resource investigations are being conducted on the Tongtianmiao pluton. Lithium-rich mica minerals serve as the predominant hosts for Li ore minerals in the area [35]. Enhanced greisenization is correlated with increased mineralization. Leveraging its distinct geological background

and mineralization conditions, the Tongtianmiao pluton has emerged as an ideal location for the study of granite-type lithium deposits.

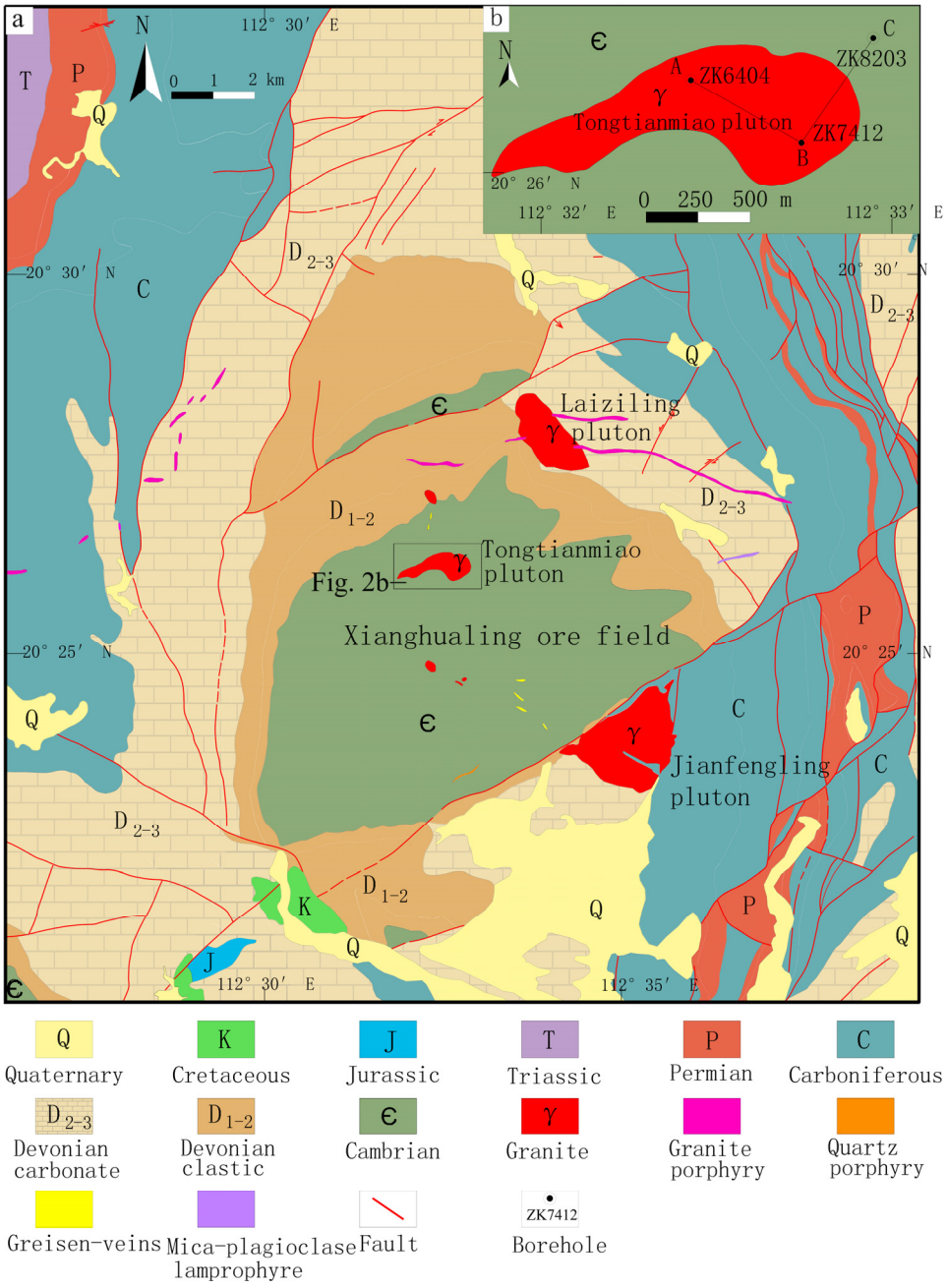

Figure 2. (**a**) Geological sketch showing the strata and intrusion distribution in the Xianghualing ore field (modified from Yuan et al., 2008 [14]); (**b**) geological sketch showing the horizontal distribution of sampling boreholes ZK6404, ZK7412 and ZK8203, CRS: WGS84.

The Tongtianmiao pluton is produced in the shape of an intrusive stock, with a total exposed area of approximately 0.6 km^2. It is accompanied by various small dykes and veins connected at depth, forming a semihidden large pluton. The Tongtianmiao pluton exhibits a vertical lithological variation: the shallower sections are predominantly medium- to fine-grained zinnwaldite granite, whereas the deeper sections consist mainly of medium-grained biotite granite and medium-grained biotite monzonitic granite, which are the ore-forming mother rocks of the mining area. The rocks are grayish white and light flesh red, with their mineral components mainly consisting of potassium feldspar, plagioclase

and quartz, followed by zinnwaldite, biotite and topaz. The mineral composition varies due to different depths of intrusion and different rock types. The rock texture is mainly medium- to fine-grained, with a few being fine-grained and a few being porphyraceous. Different types of rocks exhibit certain transitional changes in mineral composition and are subject to varying degrees of alteration, including albitization, greisenization, chloritization and kaolinization (Figure 3).

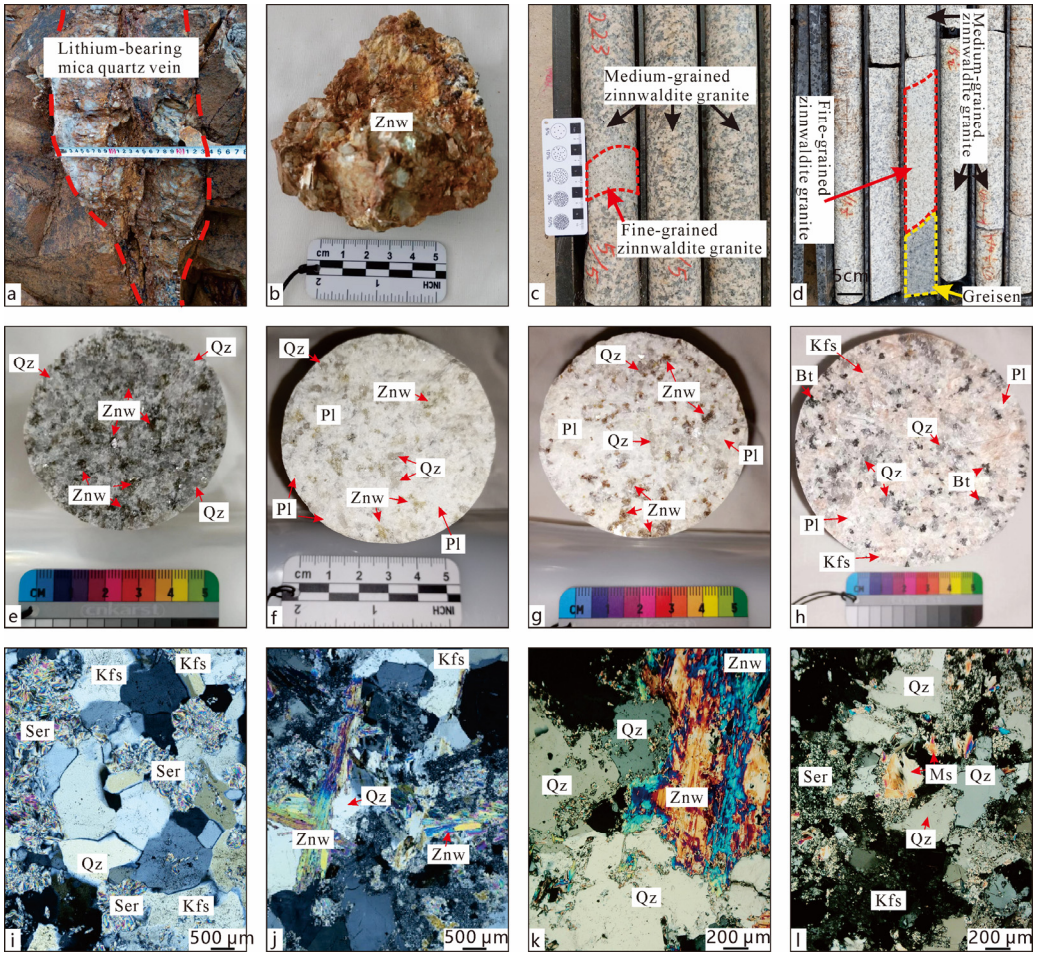

Figure 3. Photographs and micrographs of representative rocks: (**a**) lithium-rich mica quartz vein; (**b**) zinnwaldite specimen; (**c**) fine-grained zinnwaldite granite veins intersecting medium-grained zinnwaldite granite; (**d**) grain size variation and greisen vein in zinnwaldite granite; (**e**) greisen; (**f**) albitized zinnwaldite granite; (**g**) zinnwaldite granite; (**h**) biotite monzonitic granite; (**i**) sericitized granite thin section; (**j**) zinnwaldite granite thin section; (**k**) greisen thin section; (**l**) altered quartz-enriched granite thin section. Pl—plagioclase, Kfs—potassium feldspar, Qz—quartz, Znw—zinnwaldite, Ms—muscovite, Bt—biotite, Ser—sericite.

According to the type of alteration, mineral combination, and spatial distribution, the pluton can be divided from bottom to top into the biotite monzonitic granite zone, two-mica monzonitic granite zone, zinnwaldite granite zone, and greisen zone, which present the following variation patterns:

(1) Mica mineral compositions are graded from biotite, through protolithionite, zinnwaldite, lepidolite, muscovite, and finally sericite, reflecting a progressive evolutionary trend;
(2) The albite content initially increases (in the zinnwaldite granite zone) and subsequently decreases, with the upper portions undergoing progressive alteration kaolinite, sericite, and illite (in the greisen zone);

(3) The content of accessory minerals gradually increases, among which tantalite and niobite are mostly enriched in the albitized zinnwaldite granite zone, while the greisen zone is characterized by the enrichment of tungsten, cassiterite, and arsenopyrite.

3. Samples and Analytical Techniques

In this study, whole-rock major and trace element analysis samples and geochronology samples were collected from the Tongtianmiao pluton through drill cores (Figures 2 and 4). Samples ZK6404-1 to ZK6404-5, ZK8203-7, and ZK8203-8 were collected from zinnwaldite granite. Samples ZK6404-6 to ZK6404-8 were obtained from monzonitic granite, while ZK8203-5 and ZK8203-6 were from altered granite. ZK8203-9 and ZK8203-10 were sourced from albite granite, ZK8203-13 and ZK8203-15 from protolithionite K-feldspar granite, and ZK8203-4 from a lithium mica-bearing quartz vein. Sample ZK7412-1 was obtained from medium-grained zinnwaldite granite, and samples ZK7412-5 and ZK7412-6 were collected from medium- to coarse-grained biotite monzonitic granite. These samples are representative of the typical granites in the study area.

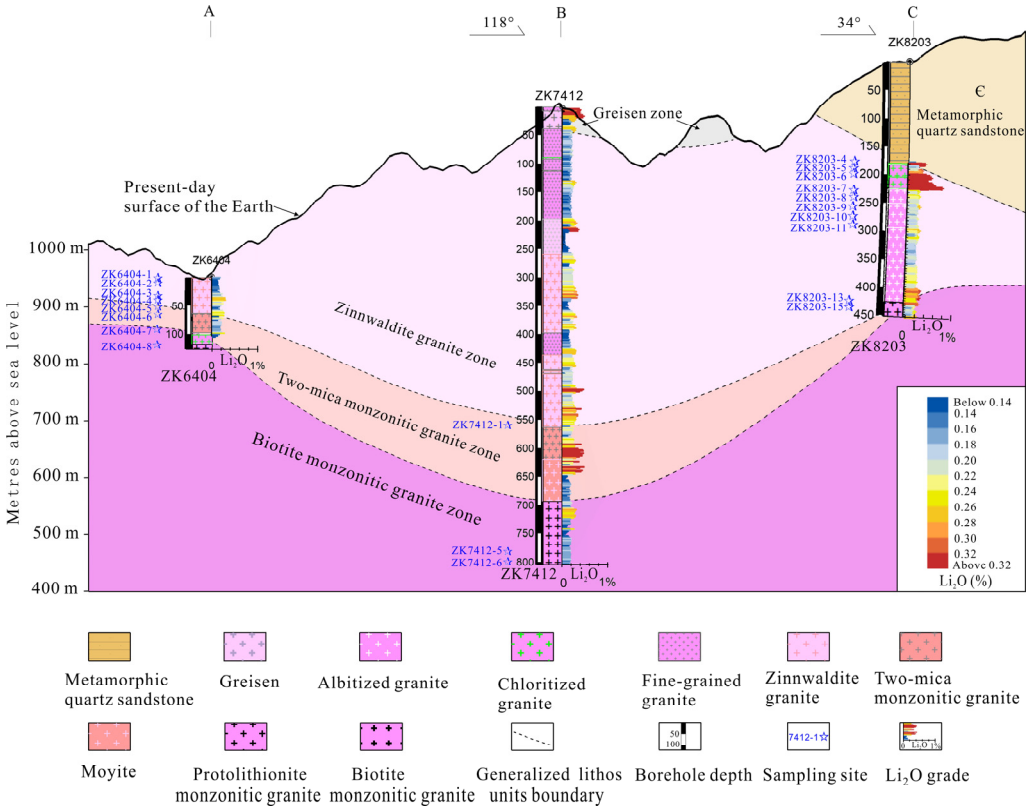

Figure 4. Geologic cross sections of drill holes ZK6404, ZK7412 and ZK8203 showing the spatial relationships among different rocks and sampling locations.

3.1. Whole-Rock Major and Trace Element Analysis

For this study, whole-rock major and trace element analyses were conducted at the ALS Minerals Laboratory in Guangzhou, China. The samples were crushed in a milling machine to pass through a 200-mesh sieve, which corresponds to a particle size of approximately 74 µm. The loss on ignition (LOI) was determined by calcining an additional portion of the dried sample in an oxygen atmosphere at 1000 °C, followed by cooling and precise reweighing. The weight difference before and after calcination represents the LOI, which is crucial for assessing the volatile components of the samples.

Major elements were analyzed using X-ray fluorescence spectrometry (ME-XRF26F). After high-temperature fusion at 1050 °C to form a glass disc, the samples were analyzed using a PANalytical PW5400, ensuring the precision and accuracy of the analysis. The

precision and accuracy are both controlled within a relative deviation (RD) of <5% for XRF and <5% for LOI.

Trace elements such as Be, Li, Pb, Sc, and Zn were analyzed using the ME-MS61r method, which combines inductively coupled plasma-optical emission spectrometry (ICP-OES) with mass spectrometry (ICP-MS). The samples were digested with a mixture of perchloric acid, nitric acid, hydrofluoric acid, and hydrochloric acid, followed by dilution with hydrochloric acid. The precision and accuracy of this method are both controlled within a relative deviation and relative error of <10%.

The analysis of Ba, Cr, Nb, Rb, Sn, Sr, Ta, Th, U, V, W, Zr, and other rare-earth elements (REEs) was performed using the ME-MS81g method, a fusion ICP-MS analytical technique. The samples were mixed with lithium borate flux buffer, mixed at 1025 °C, cooled, and digested with nitric acid, hydrochloric acid, and hydrofluoric acid before analysis using an Agilent 7900 ICP-MS system, ensuring accurate determination of refractory and rare-earth elements. The precision and accuracy of this method are similarly controlled within a relative deviation and relative error of <10%.

3.2. Zircon U–Pb Dating

High-spatial-resolution (5 μm) zircon U–Pb dating was performed using femto laser ablation-multicollector inductively coupled plasma–mass spectrometry (FSLA–MC–ICP–MS) employing a Neptune XT MC–ICP–MS instrument (Thermo Fisher Scientific, Dreieich, Germany) coupled to a 257 nm NWR-Femto laser ablation system (NWRFemtoUC, Elemental Scientific Lasers, Bozeman, MT, USA) at the Southern Marine Science and Engineering Guangdong Laboratory (Zhuhai, China). The details of the measurement procedures and calibration technique can be found in Wu et al. (2020) [36]. A laser with a diameter of 5 μm, a 3 Hz repetition rate and an energy density of ~3.0 J/cm2 was used. The Neptune XT is equipped with a so-called "jet interface", comprising a jet sample cone, an X-version skimmer cone and a high-capacity vacuum pump (OnTool Booster 150, Asslar, Germany). This leads to signal enhancement in laser sampling mode by a factor of 3–5, resulting in an improved detection capability. Helium was employed as ablation gas to improve the transport efficiency of the ablated aerosols. Standard zircon 91500 was used as the primary calibration material. The reference zircon Plěsovice [37] was analyzed as a quality control material. The accuracy and precision of the weighted mean $^{206}Pb/^{238}U$ ages are better than 2% for 5 μm spots.

3.3. Monazite U–Pb Dating

High-spatial-resolution (10 μm) U–Pb dating of the monazite was performed using the same instruments and methods as those used for zircon U–Pb dating. Due to the lower uranium content of monazite compared to that of zircon, the laser beam spot size was 10 μm to ensure sufficient signal intensity. The accuracy and precision of weighted mean $^{206}Pb/^{238}U$ ages are better than 2% for 10 μm spots. The experiment was also performed at the Southern Marine Science and Engineering Guangdong Laboratory (Zhuhai), China.

4. Results

4.1. Whole-Rock Major and Trace Elements

The whole-rock major and trace element compositions of the Tongtianmiao granites are listed in Table S1.

In terms of major element composition, there are variations in the chemical compositions among the various samples. The Tongtianmiao granitic samples are characterized by variable SiO_2 contents (69.18–78.20 wt.%, average = 74.08 wt.%) (Figure 5), high Al_2O_3 contents (11.97–17.84 wt.%, average = 14.83 wt.%) (Figure 5a), TFe_2O_3 contents (0.47–2.42 wt.%, average = 0.92 wt.%) (Figure 5b), relatively consistent MnO contents (0.04–0.20 wt.%, average = 0.10 wt.%) (Figure 5c) and MgO contents (0.02–0.22 wt.%, average = 0.07 wt.%) (Figure 5d), variable and high CaO contents (0.07–0.74 wt.%, average = 0.37 wt.%) (Figure 5e), Na_2O contents (0.03–4.32 wt.%, average = 2.73 wt.%) (Figure 5f), and K_2O contents

(0.2.82–5.44 wt.%, average = 4.13 wt.%), and low TiO_2 and P_2O_5 (less than 0.01 wt.%) (Table S1).

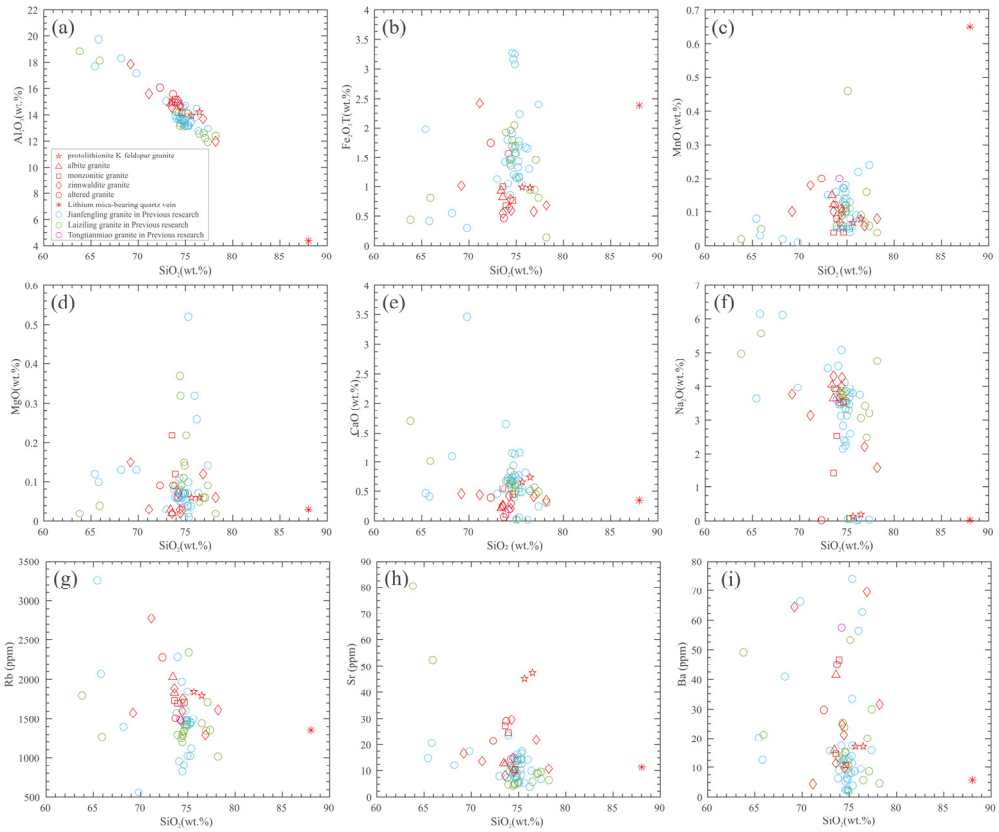

Figure 5. Plots of SiO_2 vs. (**a**) Al_2O_3; (**b**) $Fe_2O_3{}^T$; (**c**) MnO; (**d**) MgO; (**e**) CaO; (**f**) Na_2O; (**g**) Rb; (**h**) Sr; and (**i**) Ba for the Tongtianmiao granitic rocks and other intrusions in the Xianghualing ore field (data obtained from previous research [7,8,11,18]).

In terms of trace element composition, the Tongtianmiao granitic rocks exhibit high Rb contents (1300–2780 ppm) (Figure 5g) but low Sr contents (8.10–47.40 ppm) (Figure 5h) and Ba contents (4.60–69.60 ppm) (Figure 5i).

In the TAS diagrams, all samples are plotted in the subalkaline field. A sample from a lithium mica-bearing quartz vein is plotted in the quartzolite field. One sample was obtained from an altered granite plot in the granodiorite field, two samples were obtained from a zinnwaldite granite plot on the boundary between the granite field and the granodiorite field, and the remaining samples were obtained from a Tongtianmiao granite plot in the granite field (Figure 6). These granites are also rich in K_2O, and most samples plot in the calc-alkaline field and high-K calc-alkaline field, except for sample ZK6404-8, which is plotted in the shoshonite series and is near the high-K calc-alkaline series boundary (Figure 7a). The A/CNK ratios of these samples are greater than one, and the samples are classified as peraluminous granites (Figure 7b).

A shown in the primitive mantle-normalized diagram (Figure 8a), the Tongtianmiao granites samples are enriched in Rb, Nb, Zr, Hf, Ta and the majority of rare-earth elements (REEs) but are depleted in Ba, Sr, etc. In addition, the chondrite-normalized REE patterns of the Tongtianmiao granites are generally consistent with the chondrite-normalized REE patterns of the Jianfengling granites and Laiziling granites. However, the chondrite-normalized REE patterns display noticeable variations among different granite types. The ΣREE content of Tongtianmiao granites is less than the ΣREE content of Jianfengling granites and Laiziling granites. The sample from the lithium mica-bearing quartz vein has a low ΣREE content (12.63 ppm). The samples from the Tongtianmiao granites display a broad range of ΣREE contents (36.76–328.37 ppm, average = 152.81 ppm). Among them,

the samples from altered granite have low ΣREE contents (36.76 ppm and 39.88 ppm). All samples from the Tongtianmiao granites have strong negative Eu anomalies and weak positive Ce anomalies (δCe = 1.11–1.41, average = 1.22), and the fractionation of light and heavy REEs is not obvious (average LREE/HREE = 4.00 and average La_N/Yb_N = 1.81) (Figure 8b).

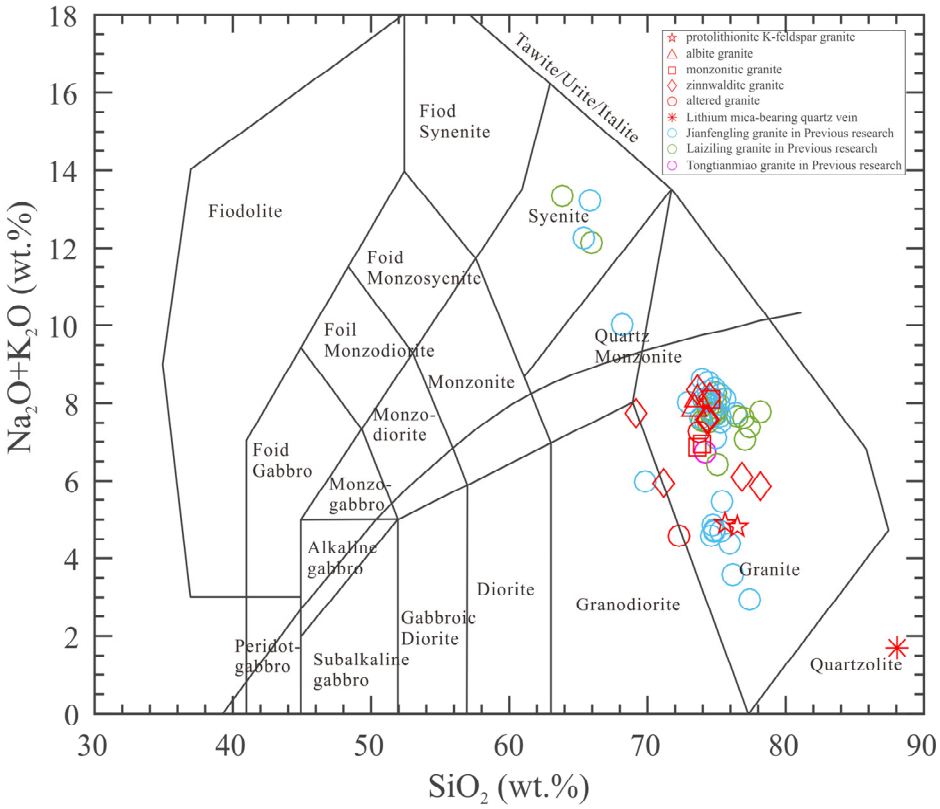

Figure 6. Chemical classification of Tongtianmiao plutonic rocks using the total alkali versus silica (TAS) diagram, modified from Middlemost (1994) [38].

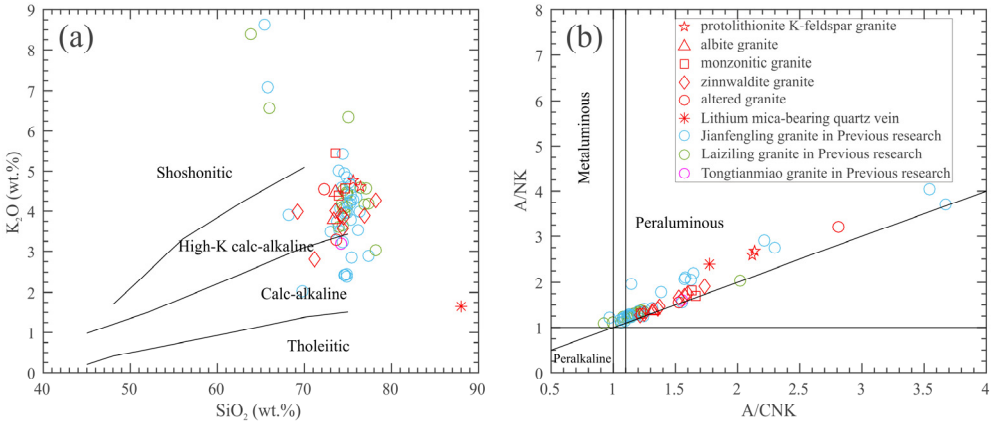

Figure 7. (**a**) SiO_2 vs. K_2O diagram, modified from Peccerillo and Taylor (1976) [39]; (**b**) A/CNK versus A/NK plots of granites from the Tongtianmiao pluton, based on the diagram of Maniar and Piccoli (1989) [40].

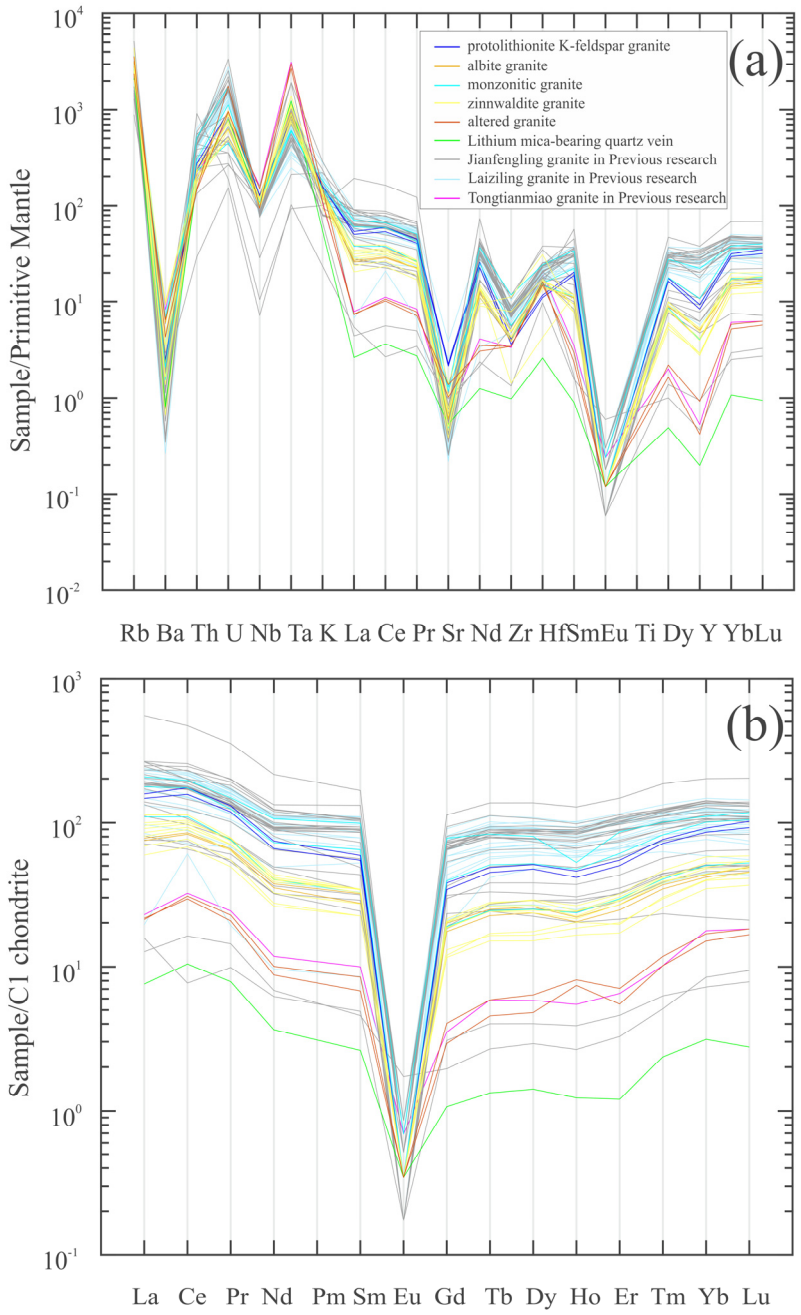

Figure 8. (**a**) The primitive mantle normalized diagram of trace elements and (**b**) the chondrite-normalized REE patterns, with normalization values from Sun and McDonough (1989) [41].

4.2. Zircon U–Pb Geochronology

Single-grain zircons selected from the zinnwaldite granite of the Tongtianmiao granite samples show distinct characteristics in CL images (Figure 9). There are two types of zircon grains in the samples according to their CL image characteristics: grains showing wide oscillatory zoning and those of the other type. The majority of the zircon grains exhibit a dark color and display weak oscillatory zoning, while a few zircons have inherited cores or marginal accretion (Figure 9).

In this study, zircons from Tongtianmiao granite samples with high U (1334–87333 ppm, average = 25,411 ppm) and Th (74–86,754 ppm, average = 6551 ppm) and low Th/U (0.06–0.99, average = 0.24) ratios (Table S2) suggest that the zircon lattice of the Tongtianmiao granite samples may have experienced radiation damage. In particular, the average value (25,411 ppm) of U significantly exceeds the threshold of 3000 ppm, similar to that of

zircon samples from Laiziling and Jianfengling, which suggests that the degree of radiation damage to the zircon lattice is high [11]. Therefore, these zircons cannot effectively record the crystallization age of granite. As a result, our subsequent research focused on the U–Pb geochronology of monazite.

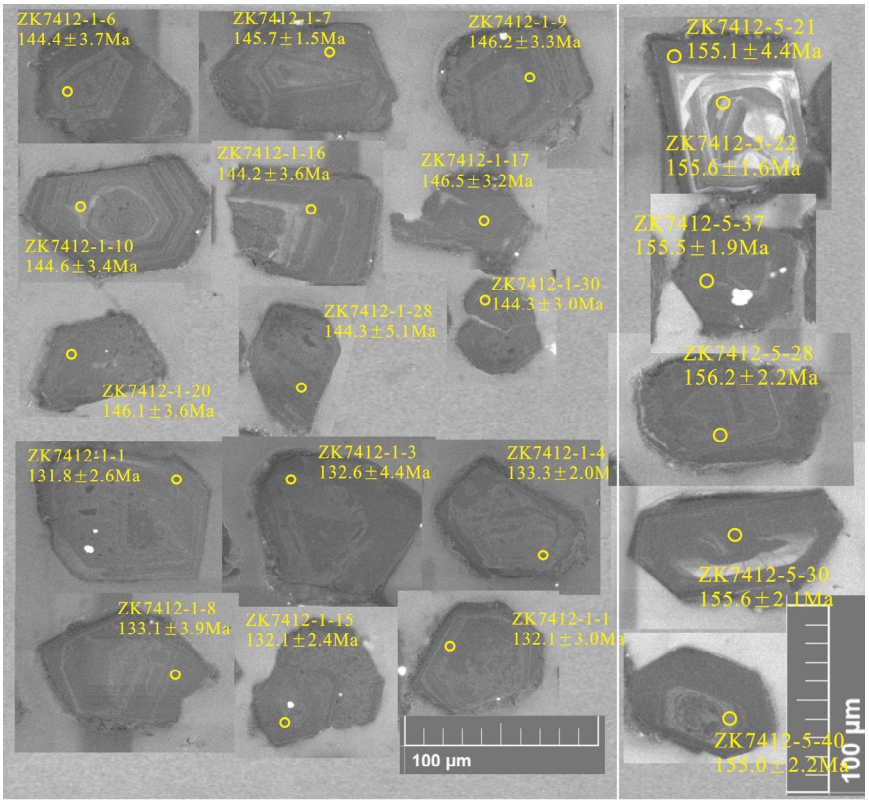

Figure 9. Zircon CL images of samples ZK7412-1 and ZK7412-5.

4.3. Monazite U–Pb Geochronology

Like high-U zircon, monazite tends to heal after radioactive damage and generally does not suffer from significant Pb loss due to severe lattice destruction [42–44]. Therefore, when zircons in rock samples are generally high in U, coexisting monazite is a more suitable alternative mineral for dating [45]. Single-grain monazite grains selected from the zinnwaldite granite in Tongtianmiao granite samples show distinct characteristics in CL images (Figure 10). The grains of monazite in the samples exhibit a range of sizes and display irregular morphologies. The composition of the monazite is uniform, and the growth zones are basically undeveloped. The Pb ages for 27 monazites are shown in Table S3. In the case of ordinary Pb content without correction, the Tera-Wasserburg antiharmonic map was drawn to obtain the lower intersection age. Monazites from granite (sample ZK7412-5) yield a lower intersection age of 167.9 ± 1.6 Ma (n = 17, MSWD = 1.1), and the weighted average age is 167.8 ± 0.2 Ma (n = 17, MSWD = 2.00) after isochronous linear ordinary lead correction (Figure 11). Monazites from granite (sample ZK7412-6) yield a lower intersection age of 172.1 ± 1.1 Ma (n = 10, MSWD = 2.1), and the weighted average age is 172.1 ± 0.5 Ma (n = 10, MSWD = 2.7) after isochronous linear ordinary lead correction (Figure 12). The weighted average $^{206}Pb/^{238}U$ ratios between 172.1 and 167.8 Ma, and the monazite U–Pb ages of the Tongtianmiao granites indicate that these granites probably formed during the Middle Jurassic.

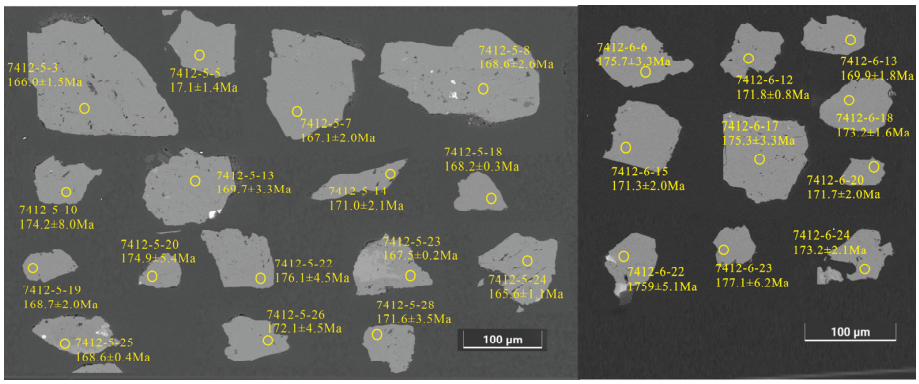

Figure 10. Monazite CL images of samples ZK7412-5 and ZK7412-6.

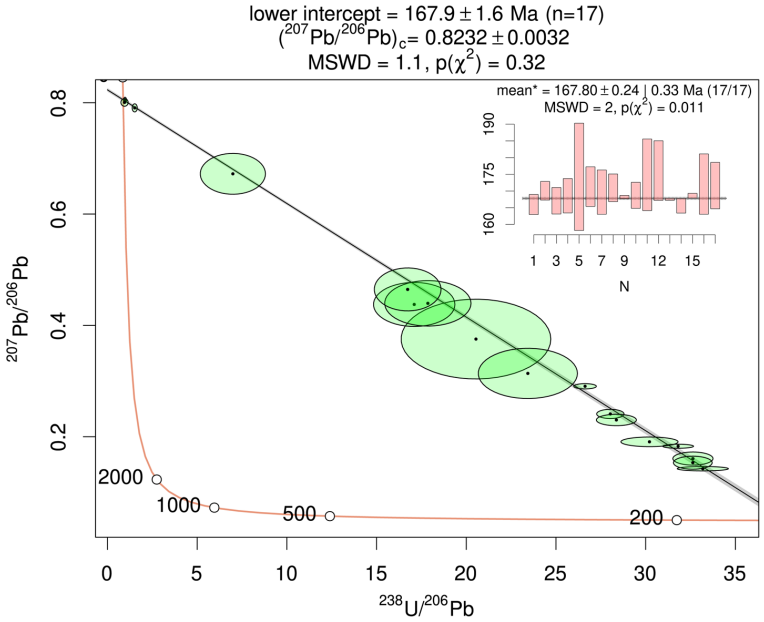

Figure 11. Monazite U–Pb ages of sample ZK7412-5.

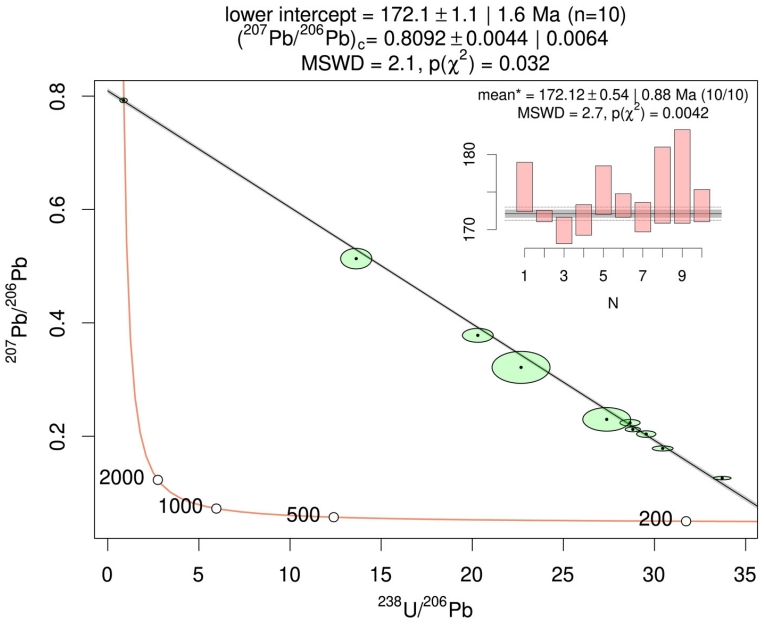

Figure 12. Monazite U–Pb ages of sample ZK7412-6.

5. Discussion

5.1. Classification and Tectonic Setting of Tongtianmiao Granites

The classification of granites has been characterized by a variety of standards, with the categorization of I-type, S-type, M-type, and A-type granites being widely recognized in the scientific community [46–56]. A-type granites are characterized by high SiO_2, K_2O, Na_2O, Zr, Nb, REE, Y, and Ga and low CaO, Sr, Ba, etc., and they are characterized by high Ga/Al and $(K_2O + Na_2O)/CaO$ [55]. The granites from Tongtianmiao are characterized by high contents of SiO_2 (69.18–78.20 wt.%, average = 74.08 wt.%) and $K_2O + Na_2O$ (4.59–8.34 wt.%, average = 6.86 wt.%), and some of the Tongtianmiao granites (especially the zinnwaldite granites ZK8203-7 and ZK8203-8) exhibit high Ga contents, with depletions in Ba, Sr, Eu, Ti and P, which are similar to the major and trace element compositions of A-type granites [55]. There are Jianfengling and Laiziling granites near the Tongtianmiao pluton, and some of the samples from these granites have geochemical characteristics similar to those of the Tongtianmiao granites (Figures 5–8 and 13). In the granite discrimination diagrams (Figure 13), Tongtianmiao granites exhibit high 10,000 Ga/Al ratios, and all samples plot in the A-type granite field; almost no granite samples plot in the I-type and/or S-type granite field in the discrimination diagrams.

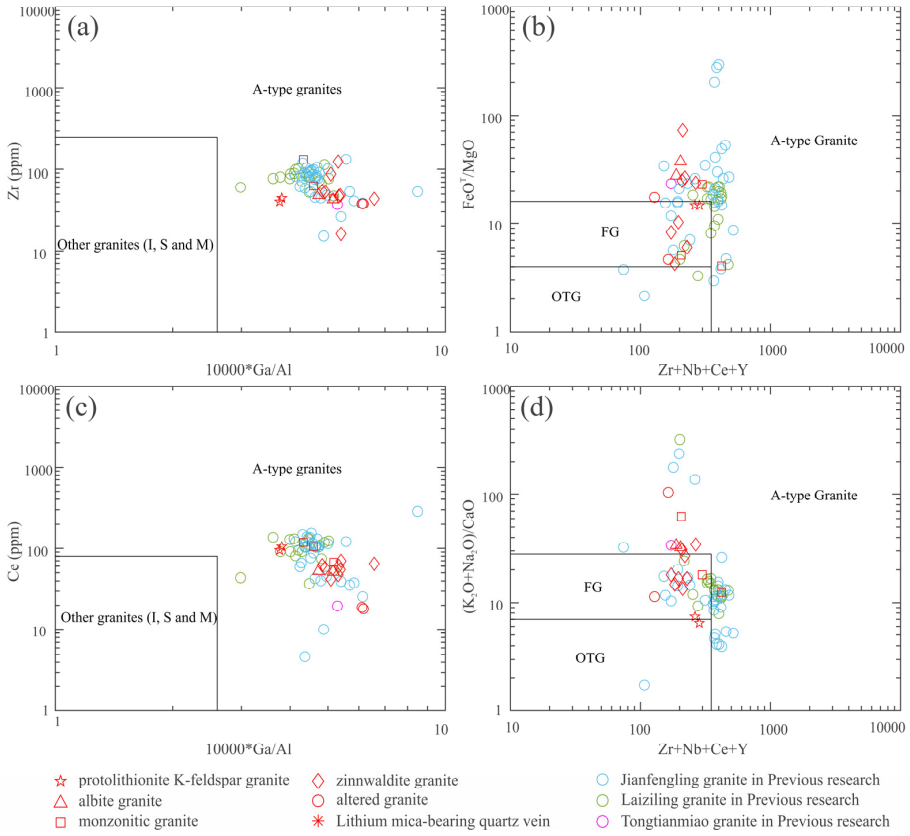

Figure 13. Granite discrimination diagram of granite genetic type (modified from [55]): (**a**) 10,000 Ga/Al vs. Zr; (**b**) Zr + Nb + Ce + Y vs. FeO^T/MgO; (**c**) 10,000 Ga/Al vs. Ce; (**d**) Zr + Nb + Ce + Y vs. $(Na_2O + K_2O)/CaO$. FG—fractionated felsic granite; OTG—other I-, S- and M-type granite.

In addition, the Tongtianmiao granites contain extremely low levels of P_2O_5 (less than 0.01 wt.%), which indicates a lack of affinity for S-type granites, and all the samples are peraluminous, exhibiting high A/CNK values (1.22–2.81, average = 1.61) higher than 1.2, further suggesting a lack of affinity for I-type granites (Figure 7). Furthermore, the Tongtianmiao granites are distinguished by high $Fe_2O_3{}^T$, K_2O, and Na_2O contents and low MgO contents, revealing that they are highly similar to A-type granites. Previous studies have indicated that the majority of Late Mesozoic granitic plutons in the Nanling region, in-

cluding Jianfengling [7,8,11,18], Laiziling [18], Xitian [57] and Qitianling [58], are classified as A-type granites. Some Tongtianmiao granites are plotted within the fractionated felsic granite field according to the discrimination diagrams of Zr + Nb + Ce + Y vs. FeO^T/MgO and Zr + Nb + Ce + Y vs. $(Na_2O + K_2O)/CaO$, especially for the zinnwaldite granite. These samples also have a high index of magmatic differentiation (average DI = 90.57). A-type granite has been continuously evolving since its conception [54,59], and it is still widely used by many scholars due to its unique geochemical characteristics and indications of the tectonic environment. In light of the aforementioned findings, the Tongtianmiao granites are classified as highly differentiated A-type granites.

There are three major tectonic developmental phases in the South Hunan region: the Caledonian period from the Sinian to the Cambrian; the Hercynian-Indosinian period from the Late Paleozoic to the Early Permian; and the Yanshanian period from the Late Triassic to the Cenozoic [60]. During the Indosinian period, intense tectonic activities dominated by collision and compression occurred. Subsequently, the tectonic stress gradually shifted from compression to extension in the Yanshanian period and entered a stage of extension and thinning. Magmatic activity occurred in the mid-Yanshanian period with the large-scale intrusion of basaltic magma, resulting in extensive crustal melting and mixing of crustal and mantle magmas [60]. In this study, the U–Pb ages of monazite grains reveal that the formation age of the Tongtianmiao granite ranged from approximately 172.1–167.8 Ma (Figures 11 and 12) in the mid-Yanshanian period.

The Jianfengling and Laiziling granites, as reported in previous studies [7,8,12,18,61], are classified as within-plate granites. Notably, the Laiziling and Jianfengling granites exhibit extremely similar elemental and Lu–Hf isotopic compositions, with high SiO_2, Al_2O_3, Na_2O, and K_2O contents and high A/CNK ratios [7]. Specifically, they exhibit negative εHf(t) values ranging from −3.86 to −1.38 and from −5.44 to −3.71, respectively, and old TDMC model ages ranging from 1.30 to 1.47 Ga and from 1.32 to 1.56 Ga, respectively [7]. The whole-rock Sr–Nd isotope data further support this source, with $^{87}Sr/^{86}Sr$ ratios ranging from 0.907275 to 4.181262 and $^{143}Nd/^{144}Nd$ ratios ranging from 0.512283 to 0.512326 [12]. A-type granites, which exhibit characteristics of high differentiation, are typically considered to experience decompression-induced partial melting of the lower crust occurring in an intraplate-extension tectonic setting accompanied by crust–mantle interactions. Given the isotopic characteristics of the proximal Laiziling and Jianfengling granites and considering the placement of Tongtianmiao granite samples, excluding the altered granite samples (ZK8203-05 and ZK8203-06), in the within-plate granite field of tectonic setting discrimination diagrams (Figure 14), it is reasonable to hypothesize that the Tongtianmiao granite may have originated in an analogous geodynamic setting characterized by crustal extension and thinning. However, this hypothesis requires further direct geological and geochemical analysis in the future.

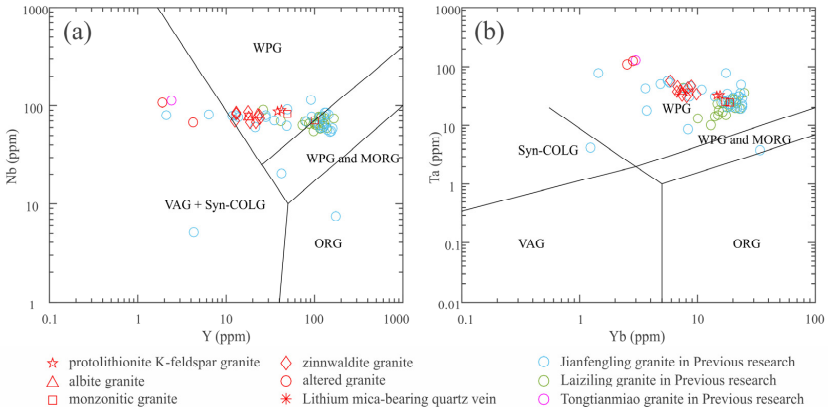

Figure 14. Granite discrimination diagram of the tectonic setting (modified from [62]): (**a**) Y vs. Nb; (**b**) Yb vs. Ta. Syn-COLG—syn-collisional granite; VAG—volcanic arc granite; ORG—ocean ridge granite; WPG—within plate granite; MORG—mantle-derived ocean ridge granite.

5.2. Petrogenesis of Tongtianmiao Granites

Tongtianmiao granites are characterized by high SiO_2 (average = 74.08 wt.%) and are classified as peraluminous (A/CNK > 1.2), and they are calc-alkaline to high-K calc-alkaline series of rocks (Figures 5 and 7). The F contents of the Tongtianmiao granites are relatively high (0.70–2.90 wt.%, average = 1.24%) (Table S1); the average F content of Jianfengling is 1.08 wt.%, and the average F content of Laiziling is 0.59 wt.% [8].

The primitive mantle normalized diagram of trace elements and the chondrite-normalized REE patterns of Tongtianmiao granites exhibit strong consistency, with the exception of three samples from a lithium mica-bearing quartz vein and altered granites (Figure 8). This consistency suggests a common genetic origin for these granites. The differences in their contents imply that they have all undergone intense crystalline differentiation and are products of different stages of evolution. Tongtianmiao granites are similar to some samples of Jianfengling and Laiziling granites in the primitive mantle-normalized diagram of trace elements and the chondrite-normalized REE patterns (Figure 8), which may imply a certain degree of similarity in their magma sources. The fractionation of light and heavy REEs is not obvious in any of the Tongtianmiao granites (average LREE/HREE = 4.00), and it is possible that late-stage F-rich fluids were more conducive to HREE enrichment [16].

The relatively consistent trace element and rare-earth element distribution patterns in the Tongtianmiao granites suggest that the magma that formed the Tongtianmiao granites may have originated from a homogeneous source region. However, granites from different parts of the pluton exhibit distinct characteristics in terms of rock types, major and trace element contents, etc. Combined with the distinct negative anomalies of Ba, Nb, Sr, Ti, and Eu, these differences might be attributed to variations in the extent of partial melting or magmatic differentiation processes. Analysis of the drill core samples reveals that the lithology of the Tongtianmiao granite exhibits a certain regularity in the vertical direction, is generally similar to that of the Jianfengling granite, and conforms to the evolution law of potassiumation–sodiumization–greisenization [8]. During the process of partial melting, light rare-earth elements (LREEs) are preferentially incorporated into the melt phase due to their higher partition coefficients in the melt. If the Tongtianmiao granites originated from varying degrees of partial melting from a common source, it would be expected that the REE content of the albite granite should be higher than that of the K-feldspar granite. However, the REE contents of the samples from the monzonitic granite, K-feldspar granite, and albite granite in the Tongtianmiao granites decrease sequentially (Table S1). During the magmatic evolution process, as fractional crystallization intensifies, the ratios of elements with similar geochemical properties exhibit regular changes. When fractional crystallization is enhanced, the K/Rb, Ba/Rb, Nb/Ta, Ni/Co, and Eu/Eu* ratios decrease, while the Rb/Sr ratio increases [63]. The K/Rb and Nb/Ta ratios of the monzonitic granites in the Tongtianmiao granites, K-feldspar granites and albite granites decrease with increasing fractional crystallization, while the Rb/Sr ratio increases with increasing fractional crystallization, indicating that the Tongtianmiao granites likely originated from fractional crystallization of the same source magma. Therefore, this study suggests that the Tongtianmiao granites can be attributed to variable degrees of fractional crystallization from a common source magma.

The trace element compositions of the Tongtianmiao granites are similar to those of crustal materials, such as negative Eu anomalies and light rare-earth element enrichment. However, Sm/Nd ranges from 0.25 to 0.30, with an average of 0.28, which is larger than that of the majority of the silicon/aluminum-rich continental crust in Nanling (0.11–0.24) [64] and close to the mantle value of 0.32 [65], indicating that it possesses characteristics of both crustal and mantle-derived granites. This is consistent with the research results that granite formed in the Yanshan Period in the southern region of Hunan contains mantle materials [8,9,66–68]. Furthermore, as a highly fractionated granite, Tongtianmiao granite is often contaminated by surrounding rocks. Therefore, the diagenetic material of the Tongtianmiao granite probably originated predominantly from the crust, with the addition of mantle-derived materials and contamination from the strata.

In the study of granites, it is widely accepted that the primary determinant affecting the diversity of granite compositions is the inherent composition of their source regions, and the effect of fractional crystallization on the diversity of granite compositions is minimal, such as for the Tuolumne batholith of the Nevada batholith in the United States [69]. However, granites of different rock types can also be formed by fractional crystallization [70]. The primary drivers of magmatic crystallization differentiation mainly include the intrinsic properties of the magma and the effects of external forces [70]. When volatiles such as H_2O and F become enriched in the residual melt, the viscosity and density of the magma continuously decrease after the onset of crystallization differentiation [71]. Specifically, volatile fluorine itself can also increase the solubility of water in granitic melts [72] and maintain a relatively high solubility even under low-pressure conditions [73]. The development of fluorine-rich micas and accessory minerals such as fluorite and topaz in the Tongtianmiao granites signifies that the residual melt in the magmatic mush system was also enriched in volatiles. A substantial number of experimental simulations and case studies have shown that deformation is an effective way to produce the through-going fractures necessary for melt migration [74,75]. The presence of various granitic dikes and veins (Figures 2 and 3) within and around the Tongtianmiao pluton indicates continuous heat supply from the base of the magma chamber, which likely facilitated the ascent of residual ore-bearing melts [6]. The provision of sustained heat is essential for in situ differentiation within the magma chamber and may have played a key role in the formation of lithium-rich granites. Additionally, the long-distance ascent experienced by granitic magma (or residual magma) during the tectonically active period of its emplacement is also an efficient mechanism for achieving its high degree of magmatic differentiation [71,76]. Affected by the retreat of the ancient Pacific subduction plate, the Middle to Late Jurassic was a period of intense activity for the NE-trending extensional fault system in the southern region of Hunan [77], and the extensional tectonics during the post-collision stage may have also provided favorable conditions for the formation of the Tongtianmiao granite. The aforementioned studies suggest that the Tongtianmiao granites could be attributed to the partial melting of crustal materials, accompanied by the underplating of mantle-derived materials and contamination from strata materials, resulting in the formation of highly differentiated granites through magmatic differentiation and the action of external forces.

6. Conclusions

(1) The Tongtianmiao granites are identified as A-type granites characterized by high SiO_2 (69.18–78.20 wt.%, average = 74.08 wt.%) and peraluminous (A/CNK > 1.2) contents.

(2) U–Pb dating of monazite from the Tongtianmiao granites indicates geological event ages ranging from 172.1 to 167.8 Ma, which corresponds to the Middle Jurassic period and is consistent with regional tectonic extensional activity.

(3) The granites exhibit a high degree of magmatic differentiation with volatile component F ranging from 0.70 to 2.90 wt.%, with an average of 1.24 wt.%. A continuous heat supply from underlying mantle-derived magma likely facilitates the ascent of residual melts. This heat is crucial for sustaining in situ differentiation within the magma chamber over time, a key process in the formation of lithium-rich granites.

(4) The timing and geodynamic setting of the Tongtianmiao granite emplacement are linked to the retreat of the Pacific subduction plate, with NE-trending extensional faults providing favorable conditions for lithium enrichment.

Supplementary Materials: The following supporting information can be downloaded at: https://www.mdpi.com/article/10.3390/min14070637/s1, Table S1: Whole-rock major and trace element compositions of the Tongtianmiao granites; Table S2: Zircon LA-ICPMS U–Pb isotopic compositions of the Tongtianmiao granites; Table S3: Monazite LA-ICPMS U–Pb isotopic compositions of the Tongtianmiao granites.

Author Contributions: Conceptualization, Y.Z. and W.C.; methodology, W.C., L.Z. and W.W.; software, H.W. and Z.W.; validation, X.Y. and W.C.; investigation, W.C., J.Y., Z.C. and Q.X.; resources, Y.Z. and Z.W.; data curation, W.C., L.Z. and W.W.; writing—original draft preparation, X.Y. and W.C.; writing—review and editing, Y.Z. and W.C.; visualization, X.Y., W.C., W.W. and C.Z.; supervision, Y.Z.; funding acquisition, Y.Z. and W.C. All authors have read and agreed to the published version of the manuscript.

Funding: This research was financially supported by the National Key Research and Development Program of China (Grant No. 2022YFF0801201), the National Natural Science Foundation of China (Grant No. U1911202), the Key-Area Research and Development Program of Guangdong Province (Grant No. 2020B1111370001), the Science and Technology Commission Project of Guangdong Province (Grant No. GDKTP2020053500), and the industry-funded collaborative research project (No. 32110-73000001) administered by Sun Yat-sen University.

Data Availability Statement: Data are available on request from the authors.

Acknowledgments: We would like to express our gratitude to Yuling Hu, Yixun Ma, Tianli Liang, et al., from the Mineral Resources Investigation Institute of Hunan Province, and Junhu Li, Hang Zhou, Zhi Liang, et al., from Hunan Dazhonghe Lithium Mining Co., Ltd., for their support in the field work, as well as to Chengxin Geological Service Company (Langfang, Hebei) and Tuoyan Geological Service Company (Guangzhou, Guangdong) for their support in sample processing. We are very grateful to all the editors and reviewers who helped us improve and publish this paper.

Conflicts of Interest: Qinghe Xu serves as an employee of Hunan Dazhonghe Lithium Mining Company Ltd. It is important to clarify that the mere existence of such a relationship or involvement in related activities does not inherently suggest a biased or problematic influence on the content of any academic paper he contributes to. However, we recognize that readers have the right and responsibility to make their own informed judgments regarding the relevance and potential impact of his relationships and activities on the content of any specific paper.

References

1. Bartels, A.; Behrens, H.; Holtz, F.; Schmidt, B.C. The effect of lithium on the viscosity of pegmatite forming liquids. *Chem. Geol.* **2015**, *410*, 1–11. [CrossRef]
2. Sirbescu, M.L.C.; Nabelek, P.I. Crystallization conditions and evolution of magmatic fluids in the Harney Peak Granite and associated pegmatites, Black Hills, South Dakota—Evidence from fluid inclusions. *Geochim. Cosmochim. Acta* **2003**, *67*, 2443–2465. [CrossRef]
3. Che, X.D.; Linnen, R.L.; Wang, R.C.; Aseri, A.; Thibault, Y. Tungsten solubility in evolved granitic melts: An evaluation of magmatic wolframite. *Geochim. Cosmochim. Acta* **2013**, *106*, 84–98. [CrossRef]
4. Toplis, M.; Dingwell, D. The variable influence of P2O5 on the viscosity of melts of differing alkali/aluminium ratio: Implications for the structural role of phosphorus in silicate melts. *Geochim. Cosmochim. Acta* **1996**, *60*, 4107–4121. [CrossRef]
5. Tang, Y.; Qin, S.X.; Zhao, J.Y.; Lü, Z.H.; Liu, X.Q.; Wang, H.; Chen, J.Z.; Zhang, H. Solubility of rare metals as a constraint on mineralization of granitic pegmatite. *Earth Sci. Front.* **2022**, *29*, 81–92. [CrossRef]
6. Guo, C.L.; Zhang, B.W.; Zheng, Y.; Xu, J.Q.; Zhao, Q.Q.; Yan, J.Y.; Zhou, R.; Fu, W.; Huang, K. Granite-type lithium deposits in China: Important characteristics, metallogenic conditions, and genetic mechanism. *Acta Pet. Sin.* **2024**, *40*, 347–403. [CrossRef]
7. Yang, L.Z.; Wu, X.B.; Cao, J.Y.; Hu, B.; Zhang, X.W.; Gong, Y.S.; Liu, W.D. Geochronology, Petrology, and Genesis of Two Granitic Plutons of the Xianghualing Ore Field in South Hunan Province: Constraints from Zircon U-Pb Dating, Geochemistry, and Lu-Hf Isotopic Compositions. *Minerals* **2018**, *8*, 213. [CrossRef]
8. Cheng, Y.S.; Mao, C.W.; Zhang, Z.W.; Xu, Z.B.; Wan, F.L.; Huang, J.Z.; Chen, J.F.; Cao, C.H.; Wen, C.H.; Zhou, Y.; et al. Petrogenesis and diagenetic dynamic background of granitic magmas in Jianfengling, Southern Hunan and its significance for rare metals mineralization. *J. Cent. South Univ. (Sci. Technol.)* **2023**, *54*, 3518–3534. [CrossRef]
9. Qiu, R.Z.; Deng, J.F.; Cai, Z.Y.; Zhou, S.; Chang, H.L.; Du, S.H. Nd isotopic characteristics and genesis of Xianghualing 430 granitic body, Hunan Province. *Acta Petrol. Mineral.* **2003**, *22*, 41–46. [CrossRef]
10. Yu, F.; Shu, Q.H.; Niu, X.D.; Xing, K.; Li, L.L.; Lentz, D.R.; Zeng, Q.W.; Yang, W.J. Composition of Garnet from the Xianghualing Skarn Sn Deposit, South China: Its Petrogenetic Significance and Exploration Potential. *Minerals* **2020**, *10*, 456. [CrossRef]
11. Yuan, L.L.; Wang, Y.F.; Liu, J.P.; Shao, Y.J.; Liu, Z.F.; Li, B.; Zheng, X.; Ding, T.; Zhang, T.D. Petro-geochemistry of Late Jurassic highly fractionated granites in the Xianghualing area of Hunan Province: Constraints on petrogenesis and rare -metal mineralization. *Acta Pet. Sin.* **2022**, *38*, 2113–2138. [CrossRef]
12. Li, H.; Wu, J.H.; Evans, N.J.; Jiang, W.C.; Zhou, Z.K. Zircon geochronology and geochemistry of the Xianghualing A-type granitic rocks: Insights into multi-stage Sn-polymetallic mineralization in South China. *Lithos* **2018**, *312*, 1–20. [CrossRef]
13. Wang, K.X.; Zhai, D.G.; Williams-Jones, A.E.; Li, D.F.; Liu, J.J. Discrete late Jurassic Sn mineralizing events in the Xianghualing Ore District, South China: Constraints from cassiterite and garnet U-Pb geochronology. *Am. Miner.* **2023**, *108*, 1384–1398. [CrossRef]

14. Yuan, S.D.; Peng, J.T.; Hu, R.Z.; Li, H.M.; Shen, N.P.; Zhang, D.L. A precise U-Pb age on cassiterite from the Xianghualing tin-polymetallic deposit (Hunan, South China). *Min. Depos.* **2008**, *43*, 375–382. [CrossRef]
15. Yuan, S.D.; Peng, J.T.; Shen, N.P.; Hu, R.Z.; Dai, T.M. 40Ar-39Ar isotopic dating of the Xianghualing Sn-polymetallic orefield in southern Hunan, China and its geological implications. *Acta Geol. Sin. Engl.* **2007**, *81*, 278–286. [CrossRef]
16. He, H.H. Mineralization Characteristics of Yanshanian Granitic Small Intrusions and Batholiths in South Hunan-Taking Qitianling and Xianghualing as Examples. Master's Thesis, Chinese Academy of Geological Sciences, Beijing, China, 2022.
17. Song, Z.F.; Yang, Q.Z.; Zhu, Z.Z.; Cao, N.W. Prospecting potential of medium-fine-grained rock-type lithium resources in the Xianghualing orefield, Hunan Province, China. *Geophys. Geochem. Explor.* **2024**, *48*, 366–374. [CrossRef]
18. Luo, Z.Y.; Li, H.; Wu, J.H.; Sun, W.B.; Zhou, J.Q.; Maulana, A. Geochronology and Geochemistry of the Xianghualing Granitic Rocks: Insights into Multi-Stage Sn-Polymetallic Mineralization in South China. *Minerals* **2022**, *12*, 1091. [CrossRef]
19. Cawood, P.A.; Zhao, G.C.; Yao, J.L.; Wang, W.; Xu, Y.J.; Wang, Y.J. Reconstructing South China in Phanerozoic and Precambrian supercontinents. *Earth-Sci. Rev.* **2018**, *186*, 173–194. [CrossRef]
20. Shu, L.S.; Yao, J.L.; Wang, B.; Faure, M.; Charvet, J.; Chen, Y. Neoproterozoic plate tectonic process and Phanerozoic geodynamic evolution of the South China Block. *Earth-Sci. Rev.* **2021**, *216*, 103596. [CrossRef]
21. Zhou, Y.Z.; Zeng, C.Y.; Li, H.Z.; An, Y.F.; Liang, J.; Lü, W.C.; Yang, Z.J.; He, J.G.; Shen, W.J. Geological evolution and ore-prospecting targets in southern segment of Qinzhou Bay-Hangzhou Bay juncture orogenic belt, southern China. *Geol. Bull. China* **2012**, *31*, 486–491. [CrossRef]
22. Mao, J.W.; Cheng, Y.B.; Chen, M.H.; Pirajno, F. Major types and time-space distribution of Mesozoic ore deposits in South China and their geodynamic settings. *Min. Depos.* **2013**, *48*, 267–294. [CrossRef]
23. Zhou, Y.Z.; Li, X.Y.; Zheng, Y.; Shen, W.J.; He, J.G.; Yu, P.P.; Niu, J.; Zeng, C.Y. Geological settings and metallogenesis of Qinzhou Bay-Hangzhou Bay orogenic juncture belt, South China. *Acta Pet. Sin* **2017**, *33*, 667–681. [CrossRef] [PubMed]
24. Zhao, Z.; Chen, Y.C.; Wang, D.H.; Li, J.K.; Liu, S.B.; Chen, Z.Y.; Guo, C.L.; Wang, P.A. Transformation of Mesozoic dynamic systems and superposition of metallogenic series of W-Sn-Li-Be-Nb-Ta-REE mineral deposits in South China. *Acta Pet. Sin.* **2022**, *38*, 301–322. [CrossRef]
25. Hu, R.Z.; Zhou, M.F. Multiple Mesozoic mineralization events in South China-an introduction to the thematic issue. *Min. Depos.* **2012**, *47*, 579–588. [CrossRef]
26. Ni, P.; Wang, G.G.; Li, W.S.; Chi, Z.; Li, S.N.; Gao, Y. A review of the Yanshanian ore-related felsic magmatism and tectonic settings in the Nanling W-Sn and Wuyi Au-Cu metallogenic belts, Cathaysia Block, South China. *Ore Geol. Rev.* **2021**, *133*, 104088. [CrossRef]
27. Zhou, M.F.; Gao, J.F.; Zhao, Z.; Zhao, W.W. Introduction to the special issue of Mesozoic W-Sn deposits in South China. *Ore Geol. Rev.* **2018**, *101*, 432–436. [CrossRef]
28. Chen, Y.C.; Pei, R.F.; Zhang, H.L.; Lin, X.D.; Bai, G.; Li, C.Y.; Hu, Y.J.; Liu, G.Q.; Xian, B.Q. *The Geology of Non-Ferrous and Rare Metal Deposits Related to Mesozoic Granitoids in Nanling Region*; Geological Publishoing House: Beijing, China, 1989; pp. 1–506.
29. Jiang, S.Y.; Su, H.M.; Xiong, Y.Q.; Liu, T.; Zhu, K.Y.; Zhang, L. Spatial-Temporal Distribution, Geological Characteristics and Ore-Formation Controlling Factors of Major Types of Rare Metal Mineral Deposits in China. *Acta Geol. Sin. Engl.* **2020**, *94*, 1757–1773. [CrossRef]
30. Wu, F.Y.; Guo, C.L.; Hu, F.Y.; Liu, X.C.; Zhao, J.X.; Li, X.F.; Qin, K.Z. Petrogenesis of the highly fractionated granites and their mineralizations in Nanling Range, South China. *Acta Pet. Sin.* **2023**, *39*, 1–36. [CrossRef]
31. Yuan, S.D.; Williams-Jones, A.E.; Romer, R.L.; Zhao, P.L.; Mao, J.W. Protolith-related thermal controls on the decoupling of Sn and W in Sn-W Metallogenic Provinces: Insights from the Nanling region, China. *Econ. Geol.* **2019**, *114*, 1005–1012. [CrossRef]
32. Zhu, J.C.; Wang, R.C.; Lu, J.J.; Zhang, H.; Zhang, W.L.; Xie, L.; Zhang, R.q. Fractionation, Evolution, Petrogenesis and Mineralization of Laiziling Granite Pluton, Southern Hunan Province. *Geol. J. China Univ.* **2011**, *17*, 381–392. [CrossRef]
33. Qin, L.X.; Rao, C.; Lin, X.Q.; Wu, R.Q.; Wang, Q. Constraints of Lithium on the Petrogenesis and Mineralization of Granite in Xianghualing Area, Hunan Province. *Geol. J. China Univ.* **2021**, *27*, 149–162. [CrossRef]
34. Xuan, Y.S.; Yuan, S.D.; Yuan, Y.B.; Mi, J.R. Zircon U-Pb age, geochemistry and petrogenesis of Jianfengling pluton in southern Hunan Province. *Miner. Depos.* **2014**, *33*, 1379–1390. [CrossRef]
35. Qiu, R.Z.; Zhou, S.; Chang, H.L.; Du, S.H.; Peng, S.B. The evolution of Li-bearing micas from Xianghualing granites and their ore-prospecting significance in Hunan. *J. Guilin Univ. Technol.* **1998**, *18*, 49–50+53–57.
36. Wu, S.T.; Yang, M.; Yang, Y.H.; Xie, L.W.; Huang, C.; Wang, H.; Yang, J.H. Improved zircon U-Pb dating at high spatial resolution (5–16 μm) by laser ablation-single collector-sector field-ICP-MS using Jet sample and X skimmer cones. *Int. J. Mass Spectrom.* **2020**, *456*, 116394. [CrossRef]
37. Sláma, J.; Kosler, J.; Condon, D.J.; Crowley, J.L.; Gerdes, A.; Hanchar, J.M.; Horstwood, M.S.A.; Morris, G.A.; Nasdala, L.; Norberg, N.; et al. Plesovice zircon—A new natural reference material for U-Pb and Hf isotopic microanalysis. *Chem. Geol.* **2008**, *249*, 1–35. [CrossRef]
38. Middlemost, E.A.K. Naming materials in the magma/igneous rock system. *Earth-Sci. Rev.* **1994**, *37*, 215–224. [CrossRef]
39. Peccerillo, A.; Taylor, S. Rare earth elements in East Carpathian volcanic rocks. *Earth Planet. Sci. Lett.* **1976**, *32*, 121–126. [CrossRef]
40. Maniar, P.D.; Piccoli, P.M. Tectonic discrimination of granitoids. *Geol. Soc. Am. Bull.* **1989**, *101*, 635–643. [CrossRef]
41. Sun, S.S.; McDonough, W.F. Chemical and isotopic systematics of oceanic basalts: Implications for mantle composition and processes. *Geol. Soc. Lond. Spec. Publ.* **1989**, *42*, 313–345. [CrossRef]

42. Harrison, T.M.; Catlos, E.J.; Montel, J.M. U-Th-Pb dating of phosphate minerals. *Rev. Miner. Geochem.* **2002**, *48*, 523–558. [CrossRef]
43. Li, Q.L. "High-U Effect"during SIMS zircon U-Pb dating. *Bull. Mineral. Petrol. Geochem.* **2016**, *35*, 405–412. [CrossRef]
44. Seydoux-Guillaume, A.M.; Paquette, J.L.; Wiedenbeck, M.; Montel, J.M.; Heinrich, W. Experimental resetting of the U-Th-Pb systems in monazite. *Chem. Geol.* **2002**, *191*, 165–181. [CrossRef]
45. Li, Q.L.; Li, X.H.; Lan, Z.W.; Guo, C.L.; Yang, Y.N.; Liu, Y.; Tang, G.Q. Monazite and xenotime U-Th-Pb geochronology by ion microprobe: Dating highly fractionated granites at Xihuashan tungsten mine, SE China. *Contrib. Mineral. Petrol.* **2013**, *166*, 65–80. [CrossRef]
46. Chappell, B.W. Aluminium saturation in I- and S-type granites and the characterization of fractionated haplogranites. *Lithos* **1999**, *46*, 535–551. [CrossRef]
47. Chappell, B.W.; Bryant, C.J.; Wyborn, D. Peraluminous I-type granites. *Lithos* **2012**, *153*, 142–153. [CrossRef]
48. Chappell, B.W.; White, A.J.R. Two contrasting granite types. *Pac. Geol.* **1974**, *8*, 173–174.
49. Chappell, B.W.; White, A.J.R. Two contrasting granite types: 25 years later. *Aust. J. Earth Sci.* **2001**, *48*, 489–499. [CrossRef]
50. Collins, W.J.; Beams, S.D.; White, A.J.R.; Chappell, B.W. Nature and origin of A-type granites with particular reference to Southeastern Australia. *Contrib. Mineral. Petrol.* **1982**, *80*, 189–200. [CrossRef]
51. Gao, P.; Zheng, Y.F.; Zhao, Z.F. Distinction between S-type and peraluminous I-type granites: Zircon versus whole-rock geochemistry. *Lithos* **2016**, *258*, 77–91. [CrossRef]
52. King, P.L.; Chappell, B.W.; Allen, C.M.; White, A.J.R. Are A-type granites the high-temperature felsic granites? Evidence from fractionated granites of the Wangrah Suite. *Aust. J. Earth Sci.* **2001**, *48*, 501–514. [CrossRef]
53. King, P.L.; White, A.J.R.; Chappell, B.W.; Allen, C.M. Characterization and origin of aluminous A-type granites from the Lachlan Fold Belt, southeastern Australia. *J. Petrol.* **1997**, *38*, 371–391. [CrossRef]
54. Loiselle, M.C. Characteristics and origin of anorogenic granites. *Geol. Soc. Am. Bull.* **1979**, *11*, 468.
55. Whalen, J.B.; Currie, K.L.; Chappell, B.W. A-type granites: Geochemical characteristics, discrimination and petrogenesis. *Contrib. Mineral. Petrol.* **1987**, *95*, 407–419. [CrossRef]
56. Wu, Q.H.; Cao, J.Y.; Kong, H.; Shao, Y.J.; Li, H.; Xi, X.S.; Deng, X.T. Petrogenesis and tectonic setting of the early Mesozoic Xitian granitic pluton in the middle Qin-Hang Belt, South China: Constraints from zircon U-Pb ages and bulk-rock trace element and Sr-Nd-Pb isotopic compositions. *J. Asian Earth Sci.* **2016**, *128*, 130–148. [CrossRef]
57. Zhou, Y.; Liang, X.Q.; Wu, S.C.; Cai, Y.F.; Liang, X.R.; Shao, T.B.; Wang, C.; Fu, J.G.; Jiang, Y. Isotopic geochemistry, zircon U-Pb ages and Hf isotopes of A-type granites from the Xitian W-Sn deposit, SE China: Constraints on petrogenesis and tectonic significance. *J. Asian Earth Sci.* **2015**, *105*, 122–139. [CrossRef]
58. Zhao, K.D.; Jiang, S.Y.; Yang, S.Y.; Dai, B.Z.; Lu, J.J. Mineral chemistry, trace elements and Sr-Nd-Hf isotope geochemistry and petrogenesis of Cailing and Furong granites and mafic enclaves from the Qitianling batholith in the Shi-Hang zone, South China. *Gondwana Res.* **2012**, *22*, 310–324. [CrossRef]
59. Bonin, B. A-type granites and related rocks: Evolution of a concept, problems and prospects. *Lithos* **2007**, *97*, 1–29. [CrossRef]
60. Mao, J.W.; Xie, G.Q.; Li, X.F.; Zhang, C.Q.; Mei, Y.X. Mesozoic large-scale mineralization and multiple lithospheric extensions in South China. *Earth Sci. Front.* **2004**, *11*, 45–55. [CrossRef]
61. Grebennikov, A.V. A-type granites and related rocks: Petrogenesis and classification. *Russ. Geol. Geophys.* **2014**, *55*, 1354–1366. [CrossRef]
62. Pearce, J.A.; Harris, N.B.W.; Tindle, A.G. Trace Element Discrimination Diagrams for the Tectonic Interpretation of Granitic Rocks. *J. Petrol.* **1984**, *25*, 956–983. [CrossRef]
63. Zhao, Z.H. Trace element geochemistry. *Adv. Earth Sci.* **1992**, *7*, 65–66.
64. Yuan, Z.X.; Zhang, Z.Q. Sm-Nd isotopic characteristics of granitoids in the Nanling region and their petrogenetic analysis. *Geol. Rev.* **1992**, *38*, 483–490. [CrossRef]
65. Henderson, P. General geochemical properties and abundances of the rare earth elements. In *Developments in Geochemistry*; Elsevier: Amsterdam, The Netherlands, 1984; Volume 2, pp. 1–32.
66. Bai, D.Y.; Chen, J.C.; Ma, T.Q.; Wang, X.F. Geochemical characteristics and tectonic setting of Qitianling A-type granitic pluton in southeast Hunan. *Acta Petrol. Mineral.* **2005**, *24*, 255–272. [CrossRef]
67. Liu, Y. Crust-mantle interaction of Yanshanian granitic magma in Qitianling and Daoxian area southern Hunan. Ph.D. Thesis, Chinese Academy of Geological Sciences, Beijing, China, 2011.
68. Wu, G.Y. The Yanshanian Granitoids and Their Cosmical Mineralization Interaction in Poly Metallogenic Deposit-Concentrated, Area in Southeastern Hunan. Ph.D. Thesis, China University of Geosciences (Beijing), Beijing, China, 2005.
69. Coleman, D.S.; Gray, W.; Glazner, A.F. Rethinking the emplacement and evolution of zoned plutons: Geochronologic evidence for incremental assembly of the Tuolumne Intrusive Suite, California. *Geology* **2004**, *32*, 433–436. [CrossRef]
70. Wu, F.Y.; Li, X.H.; Yang, J.H.; Zheng, F.Y. Discussions on the petrogenesis of granites. *Acta Pet. Sin.* **2007**, *23*, 1217–1238. [CrossRef]
71. Wu, F.Y.; Liu, X.C.; Ji, W.Q.; Wang, J.M.; Yang, L. Highly fractionated granites: Recognition and research. *Sci. Sin.* **2017**, *47*, 745–765. [CrossRef]
72. Holtz, F.; Dingwell, D.B.; Behrens, H. Effects of F, B2O3 and P2O5 on the solubility of water in haplogranite melts compared to natural silicate melts. *Contrib. Mineral. Petrol.* **1993**, *113*, 492–501. [CrossRef]
73. Giordano, D.; Romano, C.; Dingwell, D.B.; Poe, B.; Behrens, H. The combined effects of water and fluorine on the viscosity of silicic magmas. *Geochim. Cosmochim. Acta* **2004**, *68*, 5159–5168. [CrossRef]

74. Barboni, M.; Bussy, F. Petrogenesis of magmatic albite granites associated to cogenetic A-type granites: Na-rich residual melt extraction from a partially crystallized A-type granite mush. *Lithos* **2013**, *177*, 328–351. [CrossRef]
75. Bons, P.D.; Arnold, J.; Elburg, M.A.; Kalda, J.; Soesoo, A.; van Milligen, B.P. Melt extraction and accumulation from partially molten rocks. *Lithos* **2004**, *78*, 25–42. [CrossRef]
76. Tartèse, R.; Boulvais, P. Differentiation of peraluminous leucogranites "en route" to the surface. *Lithos* **2010**, *114*, 353–368. [CrossRef]
77. Mao, J.W.; Xie, G.Q.; Guo, C.L.; Chen, Y.C. Large-scale tungsten-tin mineralization in the Nanling region, South China: Metallogenic agesand corresponding geodynamic processes. *Acta Pet. Sin.* **2007**, *23*, 2329–2338. [CrossRef]

Disclaimer/Publisher's Note: The statements, opinions and data contained in all publications are solely those of the individual author(s) and contributor(s) and not of MDPI and/or the editor(s). MDPI and/or the editor(s) disclaim responsibility for any injury to people or property resulting from any ideas, methods, instructions or products referred to in the content.